Molecular Therapy
Original Article

The long non-coding RNA *NRON* promotes the development of cardiac hypertrophy in the murine heart

Jeannine Hoepfner,[1,6] Julia Leonardy,[1,6] Dongchao Lu,[1] Kevin Schmidt,[1] Hannah J. Hunkler,[1] Sinje Biß,[1] Ariana Foinquinos,[1] Ke Xiao,[1] Kumarswamy Regalla,[1] Deepak Ramanujam,[2,3] Stefan Engelhardt,[2,3] Christian Bär,[1,4,5] and Thomas Thum[1,4,5]

[1]Institute of Molecular and Translational Therapeutic Strategies, Hannover Medical School, Carl-Neuberg-Str. 1, 30625 Hannover, Germany; [2]Institute of Pharmacology and Toxicology, Technical University Munich, 80802 Munich, Germany; [3]DZHK (German Center for Cardiovascular Research), Partner Site Munich Heart Alliance, 80802 Munich, Germany; [4]REBIRTH Center for Translational Regenerative Medicine, Hannover Medical School, 30625 Hannover, Germany; [5]Fraunhofer Institute for Toxicology and Experimental Medicine, 30625 Hannover, Germany

Physiological and pathological cardiovascular processes are tightly regulated by several cellular mechanisms. Non-coding RNAs, including long non-coding RNAs (lncRNAs), represent one important class of molecules involved in regulatory processes within the cell. The lncRNA *non-coding repressor of NFAT* (*NRON*) was described as a repressor of the nuclear factor of activated T cells (NFAT) in different *in vitro* studies. Although the calcineurin/NFAT-signaling pathway is one of the most important pathways in pathological cardiac hypertrophy, a potential regulation of hypertrophy by *NRON in vivo* has remained unclear. Applying subcellular fractionation and RNA fluorescence *in situ* hybridization (RNA-FISH), we found that, unlike what is known from T cells, in cardiomyocytes, *NRON* predominantly localizes to the nucleus. Hypertrophic stimulation in neonatal mouse cardiomyocytes led to a downregulation of *NRON*, while *NRON* overexpression led to an increase in expression of hypertrophic markers. To functionally investigate *NRON in vivo*, we used a mouse model of transverse aortic constriction (TAC)-induced hypertrophy and performed *NRON* gain- and loss-of-function experiments. Cardiomyocyte-specific *NRON* overexpression *in vivo* exacerbated TAC-induced hypertrophy, whereas cardiomyocyte-specific *NRON* deletion attenuated cardiac hypertrophy in mice. Heart weight, cardiomyocyte cell size, hypertrophic marker gene expression, and left ventricular mass showed a *NRON*-dependent regulation upon TAC-induced hypertrophy. In line with this, transcriptome profiling revealed an enrichment of anti-hypertrophic signaling pathways upon *NRON*-knockout during TAC-induced hypertrophy. This set of data refutes the hypothesized anti-hypertrophic role of *NRON* derived from *in vitro* studies in non-cardiac cells and suggests a novel regulatory function of *NRON* in the heart *in vivo*.

INTRODUCTION

Cardiovascular diseases display the most common cause of death worldwide. Long non-coding RNAs (lncRNAs) are a subtype of non-coding RNAs with a size of more than 200 nucleotides[1] and play important roles in the cardiovascular system on many different levels.[2] Hence, lncRNAs might be considered as targets for future treatment strategies. The lncRNA *Braveheart* was reported to be involved in cardiac lineage development,[3] whereas *Fendrr* is needed for the control of chromatin modification.[4] Especially the role of lncRNAs in the development of disease conditions is of high interest. For instance, *Meg3* is a cardiac-fibroblast-enriched lncRNA whose expression level decreases during the late cardiac remodeling phase after chronic pressure overload.[5] Another lncRNA, called *Chast,* was discovered to be upregulated and pro-hypertrophic in mouse hearts after transverse aortic constriction (TAC)-induced cardiac hypertrophy,[6] whereas the lncRNA *H19* was shown to have an anti-hypertrophic effect.[7] A therapy using antisense oligonucleotides to silence *Chast* and a gene therapy approach to overexpress *H19*, respectively, even prevented and attenuated pathological cardiac remodeling and thereby reinforced the therapeutic potential of ncRNA-based therapies.[8,9]

The development of pathological cardiac hypertrophy can be triggered through different derailed regulatory signaling pathways. One important pathway is the calcineurin/nuclear factor of activated T cells (NFAT)-signaling pathway. A sustained elevated level of intracellular calcium leads to the activation of calcineurin, which in turn dephosphorylates the NFAT transcription factor family.[10,11] The

Received 17 March 2021; accepted 27 November 2021;
https://doi.org/10.1016/j.ymthe.2021.11.018.

[6]These authors contributed equally

Correspondence: Christian Bär, PhD, Institute of Molecular and Translational Therapeutic Strategies, Hannover Medical School, Carl-Neuberg-Str. 1, 30625 Hannover, Germany.
E-mail: baer.christian@mh-hannover.de
Corresponding: Thomas Thum, MD, PhD, Institute of Molecular and Translational Therapeutic Strategies, Hannover Medical School, Carl-Neuberg-Str. 1, 30625 Hannover, Germany.
E-mail: thum.thomas@mh-hannover.de

activation of NFAT through dephosphorylation leads to its translocation into the nucleus, where it can induce the expression of several genes, leading to the maladaptive pro-hypertrophic response including the transcriptional switch to the fetal gene program.[12] Interestingly, it has been shown that the formation of a RNA-protein scaffold complex inhibits the action of NFAT *in vitro*. In 2005, Willingham et al. identified a lncRNA that functioned as a key repressor of NFAT in HEK293 cells and named it "noncoding repressor of NFAT (NRON)".[13] Further studies described *NRON* as a cytoplasmic scaffold for a RNA-protein complex regulating the localization and activity of NFAT in T cells.[14] To date, the exact role and mode of action of *NRON in vivo* still remain unclear. So far, *NRON* was shown to have a role in the life cycle of HIV-1,[15,16] as well as in cancer cells.[17,18] In the cardiac system, circulating *NRON* levels can serve as a biomarker for heart failure[19] and can reduce atrial fibrosis by promoting the phosphorylation of NFATc3 in fibroblasts.[20]

Since NFAT plays a crucial role in the development of cardiac hypertrophy and *NRON* was suggested as a mediator of nuclear NFAT exclusion, we now hypothesized that *NRON* acts as anti-hypertrophic lncRNA. We thus characterized the role of *NRON* in the murine cardiac system by performing loss- and gain-of-function studies in a mouse model of pressure-overload-induced heart failure.

RESULTS

NRON is enriched in cardiomyocytes and regulated during the development of pathological hypertrophy

We first investigated the subcellular distribution of *NRON* in cardiomyocytes. Using neonatal mouse cardiomyocytes (NMCMs), we found that 85.9% of *NRON* transcripts associated to chromatin, whereas only 2.19% were detected in the cytoplasmic fraction and 11.91% in the nuclear soluble fraction (Figure 1A). These data were in marked contrast to previous studies showing a cytosolic localization of *NRON* in blood-derived cells.[14] We speculated that *NRON* may play a distinct role in the cardiac system and thus further investigated its role *in vivo*. We measured *NRON* expression levels in murine heart fractions. Whole hearts from adult mice were harvested and fractionated into cardiomyocytes, endothelial cells, and fibroblasts. The expression of *NRON* was highest in cardiomyocytes and significantly lower in endothelial cells and fibroblasts (Figure 1B; cycle threshold [ct] values are given in Table S1). Since NFAT plays an important role during the development of cardiac hypertrophy, we speculated that the expression of *NRON* might be also affected by pressure-overload-induced cardiac hypertrophy *in vivo*. We measured *NRON* expression in murine heart samples 2–13 weeks after TAC and Sham surgery (Figure 1C). *NRON* levels showed a biphasic regulation with significant downregulations (early) 2 weeks and (late) 13 weeks after TAC. We next tested the role of *NRON* in primary NMCMs and exposed the cells to hypertrophic stimuli using isoprenaline and phenylephrine (100 μM) for 48 h followed by measurements of the level of known hypertrophic markers as well as from *NRON* (Figure 1D). *Brain natriuretic peptide* (*Bnp*) and *myocyte-enriched calcineurin-interacting protein* (*Mcip1.4*) were significantly upregulated, while the level of *NRON* RNA was significantly decreased. We performed copy-number qPCR to get quantitative data about *NRON* expression changes and detected 30 ± 4.7 *NRON* molecules in 500 ng total RNA in untreated NMCMs versus 24 ± 2.7 molecules in NMCMs after treatment with phenylephrine/isoprenaline (Pe/Iso) for 48 h (Figure 1E).

To further study the effect of *NRON in vitro*, we infected NMCMs with adeno-associated virus 6 (AAV6)-empty or AAV6-*NRON* viral particles at an MOI of 5×10^3 for 72 h and measured the expression of hypertrophic markers and *NRON*. Surprisingly, this led to an increase in hypertrophic markers in NMCMs (Figure 1F). To examine the effects of *NRON* overexpression in more detail, we fractionated NMCMs after viral infection and measured the distribution of *NRON*. As is already shown in Figure 1A, the majority of *NRON* is detectable as a chromatin-associated fraction. After overexpression, the largest proportion of nuclear *NRON* is still chromatin-associated. In total, the distribution is partially shifted toward the cytoplasmic fraction (Figure 1G). In addition to the assessment of *NRON* distribution in subcellular fractions of NMCMs using qPCR, we performed RNA fluorescence *in situ* hybridization (RNA-FISH) to visualize the lncRNA under basal conditions and after AAV6-*NRON* transduction. To do so, we used a *NRON*-specific probe set in NMCMs, validating the previously identified subcellular distribution obtained by fractionation and qPCR studies (Figure 1H).

These interesting findings prompted us to perform further *NRON* loss- and gain-of-function experiments in mice undergoing TAC and Sham surgery.

AAV9-mediated overexpression of *NRON* exacerbated pressure-overload-induced cardiac hypertrophy

For *NRON* gain-of-function experiments in murine hearts, we used an AAV9-cardiac troponin T (cTnT) vector to overexpress *NRON* selectively in cardiomyocytes in comparison to an empty control. After a tail vein injection of 1.5×10^{12} viral particles into adult mice and subsequent TAC surgery, we detected an overexpression of the *NRON* transcript in the murine heart (Figure 2A and S1). The effect of AAV9-mediated *NRON* overexpression on cardiac hypertrophy was measured 6 weeks after TAC or Sham surgery. As expected, the TAC surgery led to an increase in the cardiac weight of the animals. When comparing the animals that underwent TAC surgery, *NRON* overexpression led to a significant increase in heart weight as compared to AAV9-empty-treated mice (Figure 2B). This effect was even more pronounced when comparing the cardiomyocyte cross-sectional area after TAC surgery between AAV9-empty- and AAV9-*NRON*-treated mice. The cross-sectional area of the cardiomyocytes was highest in the animals that received a TAC surgery in combination with an overexpression of *NRON* (Figures 2C and 2D). To characterize the different animal groups in more detail, RNA was isolated, and the mRNA level of different cardiac hypertrophy marker genes was measured. The expression levels of *Bnp* and *Mcip1.4* were highest in TAC-operated animals treated with AAV9-*NRON* (Figures 2E and 2F). When measuring cardiac dimensions after performing echocardiographic analysis of the mice,

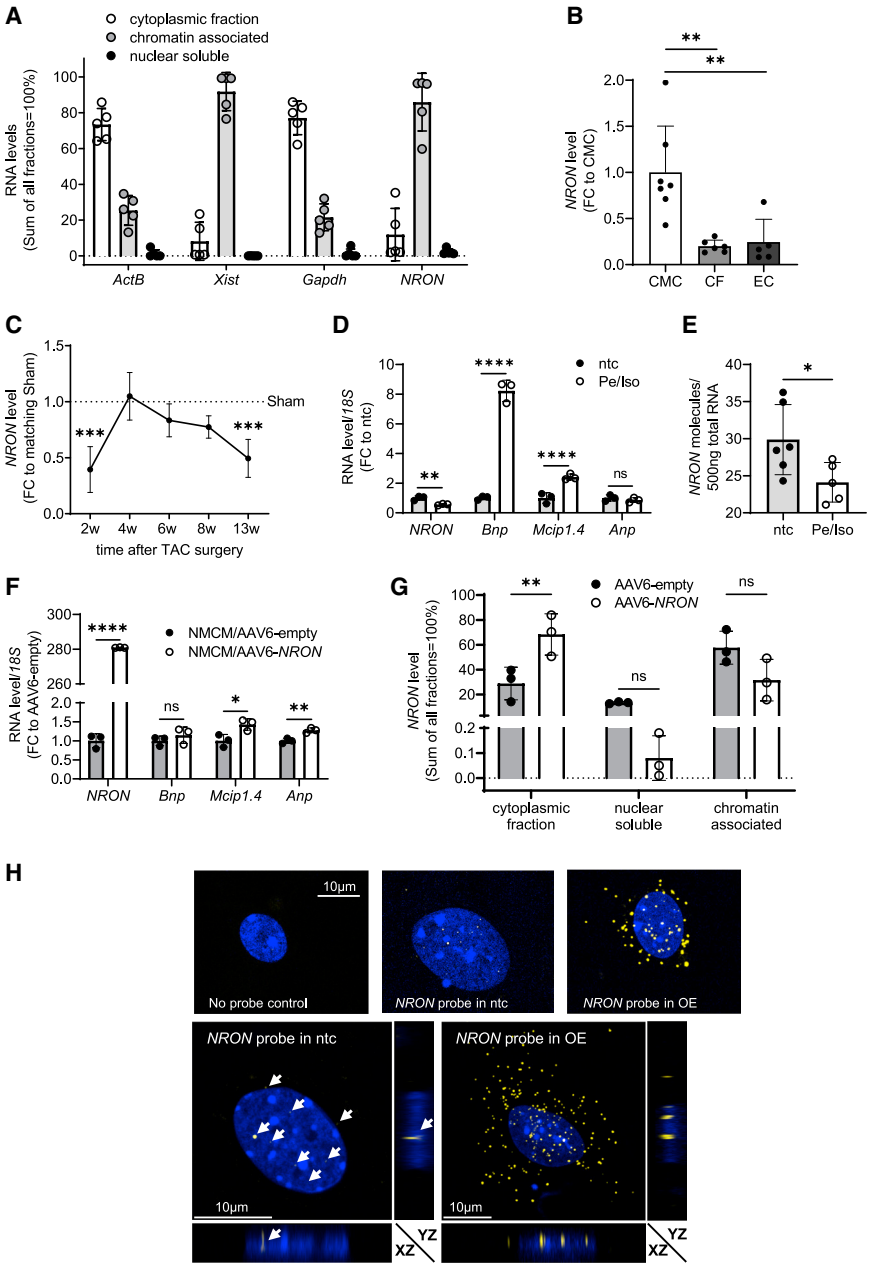

Figure 1. *NRON* level in neonatal mouse cardiomyocytes and heart fractions and after transaortic constriction

(A) Subcellular distribution of *NRON* in NMCM subfractions. *Gapdh*, *ActB*, and *Xist* mRNA levels were measured as positive controls. Data are calculated as fold change (FC) to the main fraction of the transcript measured by qPCR (mean ± SD; n = 5). (B) Distribution of *NRON* in murine heart fractions: cardiomyocytes (CMCs), cardiac fibroblasts (CFs), and endothelial cells (ECs). The expression level was measured by qPCR, and *ActB* was used as a reference gene. Data are calculated as FC to the main fraction (CMCs) of the transcript (mean ± SD; n = 5–7). **p < 0.01; one-way Anova with Tukey's multiple comparisons test. (C) The expression of *NRON* in the whole mouse heart after 2, 4, 6, 8, and 13 weeks of TAC surgery. The expression level was measured by qPCR, and *ActB* was used as a reference gene. Data are calculated relative to Sham samples of each time point (mean ± SD; n = 5–8). ***p < 0.001; one-way ANOVA with Sidak multiple comparisons test. (D) RNA levels in neonatal mouse cardiomyocytes (NMCMs) after treatment with 100 µM Pe/Iso for 48 h. The RNA level was measured by qPCR relative to *18S* RNA. The FC was calculated using the respective RNA levels in not-treated controls (ntcs). All data are mean ± SD; n = 3. *p < 0.05; **p < 0.01; ***p < 0.001; ****p < 0.0001; Student's t test. (E) Absolute quantification of *NRON* molecules in NMCMs. A plasmid standard containing murine *NRON* was used for quantification, and the level of *NRON* was measured by qPCR. NMCMs were either not treated (ntcs) or treated with 100 µM Pe/Iso for 48 h. n = 6 technical replicates. *p < 0.05; **p < 0.01; ***p < 0.001; ****p < 0.0001; Student's t test. (F) RNA levels in NMCMs after the transduction of AAV6-*NRON*. The RNA level was measured by qPCR relative to *18S* RNA. The FC was calculated using the respective RNA level in AAV6-empty-treated cells as control. All data are mean ± SD; n = 3. *p < 0.05; **p < 0.01; ***p < 0.001; ****p < 0.0001; Student's t test. (G) Subcellular distribution of *NRON* in NMCM subfractions of cells treated with 5 × 10^3 AAV6-empty or AAV6-*NRON* viral particles. Data are calculated by taking the sum of all fractions as 100% (mean ± SD; n = 3). The RNA level was measured by qPCR. *p < 0.05; **p < 0.01; ***p < 0.001; ****p < 0.0001; two-way ANOVA with Tukey's multiple comparisons test. (H) Staining of *NRON* in NMCMs using RNA-FISH. (Top panel) RNA-FISH of a single nucleus from untreated NMCMs stained with no probe as control and NMCMs infected with AAV6-empty (ntcs) or AAV6-*NRON* (overexpressed [OE]) viral particles stained with probe for *NRON*. (Bottom panel) Orthogonal sections from z stack confocal images of NMCMs infected with AAV6-empty (ntcs) or AAV6-*NRON* (OE) viral particles and stained with RNA-FISH. DAPI was used to stain the nucleus, and *NRON* was stained using an Alexa Fluor 546 tagged probe set. Representative images were taken using a confocal microscopy. Scale bar, 10 µm.

an increase in left ventricular (LV) mass in AAV9-*NRON*-treated and TAC-operated mice became apparent in comparison to AAV9-empty TAC mice (Figure 2G). The ejection fraction showed a tendency toward reduced cardiac function upon *NRON* overexpression but did not reach significance (Table S2). Thereby, these data indicate a pro-hypertrophic effect of *NRON* in the murine cardiac system.

Cardiac hypertrophy is attenuated in *NRON* KO mice

We next investigated the consequences of a *NRON* knockout *in vivo* on cardiac hypertrophy. Therefore, we generated mice with a Myh7-Cre-mediated, cardiomyocyte-specific knockout for *NRON* and verified this knockout with a phenotyping polymerase chain reaction (PCR) using the primers as depicted in Figure 3A. When comparing wild type (WT) with *NRON* knockout (KO) mice 6 and 13 weeks after

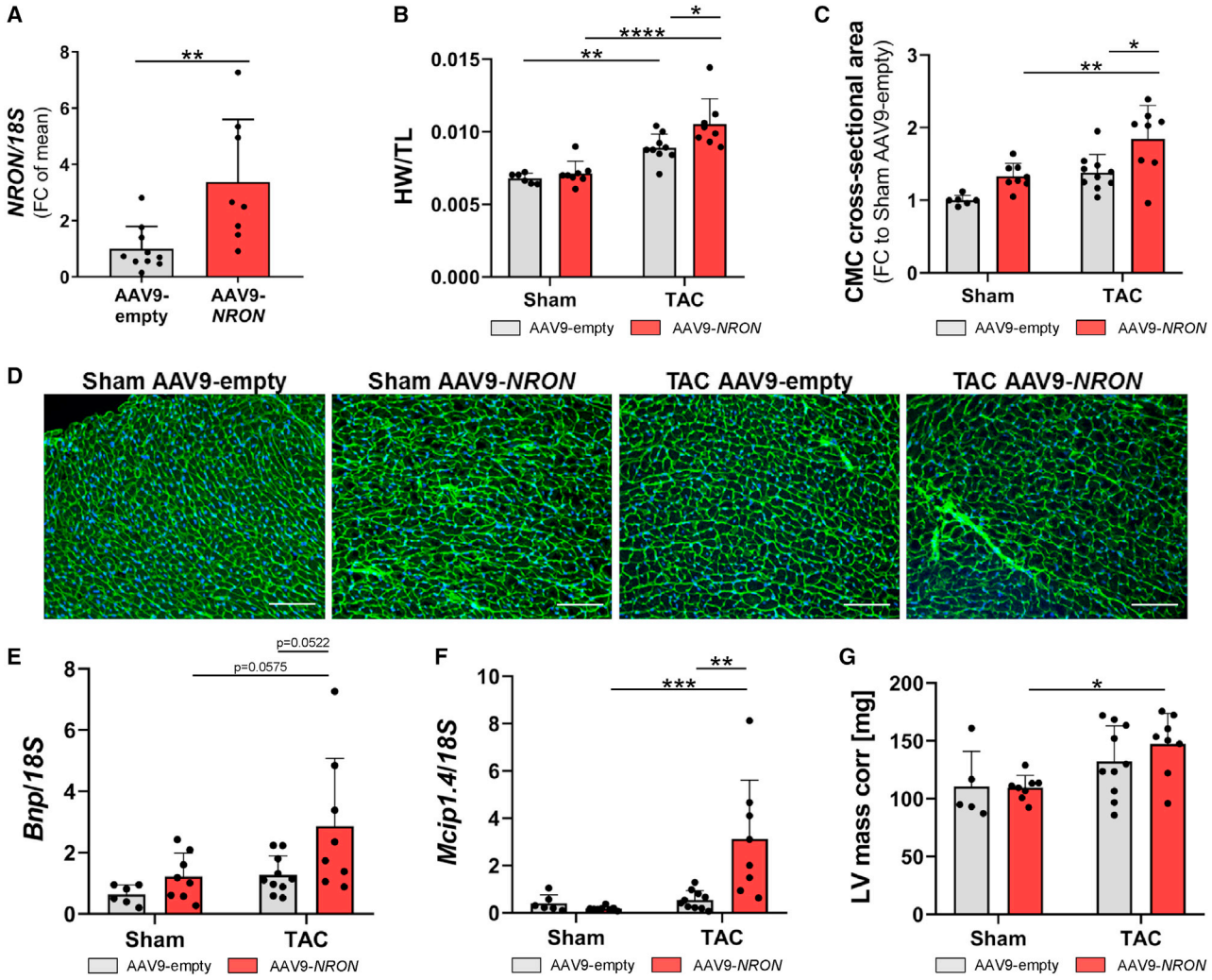

Figure 2. TAC surgery of mice after injection of AAV9-*NRON*

1.5×10^{12} AAV9-*NRON* or AAV9-empty viral particles were injected following TAC or Sham surgery. Mice were sacrificed after 6 weeks. (A) *NRON* level was measured by qPCR. (B) Heart weight (HW) was measured relative to the length of the murine tibia (TL). (C and D) The cardiomyocyte cross-sectional area was analyzed by WGA staining, and the fold change was calculated relative to Sham AAV9-empty samples. Scale bar, 100 μm. (E and F) The levels of (E) *Bnp* and (F) *Mcip1.4* mRNA were measured by qPCR relative to *18S* RNA. (G) Left ventricular mass corrected (LV mass corr) was analyzed by echocardiography. All data are mean ± SD; n = 5–10; *p < 0.05; **p < 0.01; ***p < 0.001; ****p < 0.0001; two-way ANOVA with Tukey's multiple comparisons test or Student's t test.

Sham surgery, no differences were visible regarding heart weight and the cardiomyocyte cross-sectional area (Figures 3B–3E), indicating that *NRON* is dispensable for cardiac function under homeostatic conditions.

To investigate the effect of *NRON* KO *in vivo* on the development of pressure-overload-induced cardiac hypertrophy, we performed TAC or Sham surgeries in WT and *NRON* KO mice. The mice were sacrificed 2, 6, or 13 weeks after surgery, and different cardiac parameters were measured. *NRON* KO mice exposed to 6 and 13 weeks of TAC showed a significantly lower heart weight than the respective WT mice (Figures 3B and 3C). This trend was also apparent when comparing the cardiomyocyte cross-sectional area (Figures 3D and 3E). However, no difference was detectable after 2 weeks (data not shown). When comparing the gene expression of hypertrophic markers after 6 weeks of TAC, significantly decreased expression levels of *Bnp* and *Mcip1.4* were detectable upon *NRON* KO (Figures 3F and 3G). Although less pronounced, these trends were also visible after 13 weeks of TAC (Figures 3H and 3I). Cardiac dimensions after performing echocardiographic analysis of the mice showed a lower LV mass in *NRON* KO mice 6 weeks after TAC surgery (Figure 3J). This effect was even more pronounced and significant after 13 weeks of TAC (Figure 3K; Table S3). In contrast to the gain-of-function data described above, a *NRON* loss of function resulted in an anti-hypertrophic effect in the murine cardiac system, thus corroborating a function of *NRON* in cardiovascular disease *in vivo*.

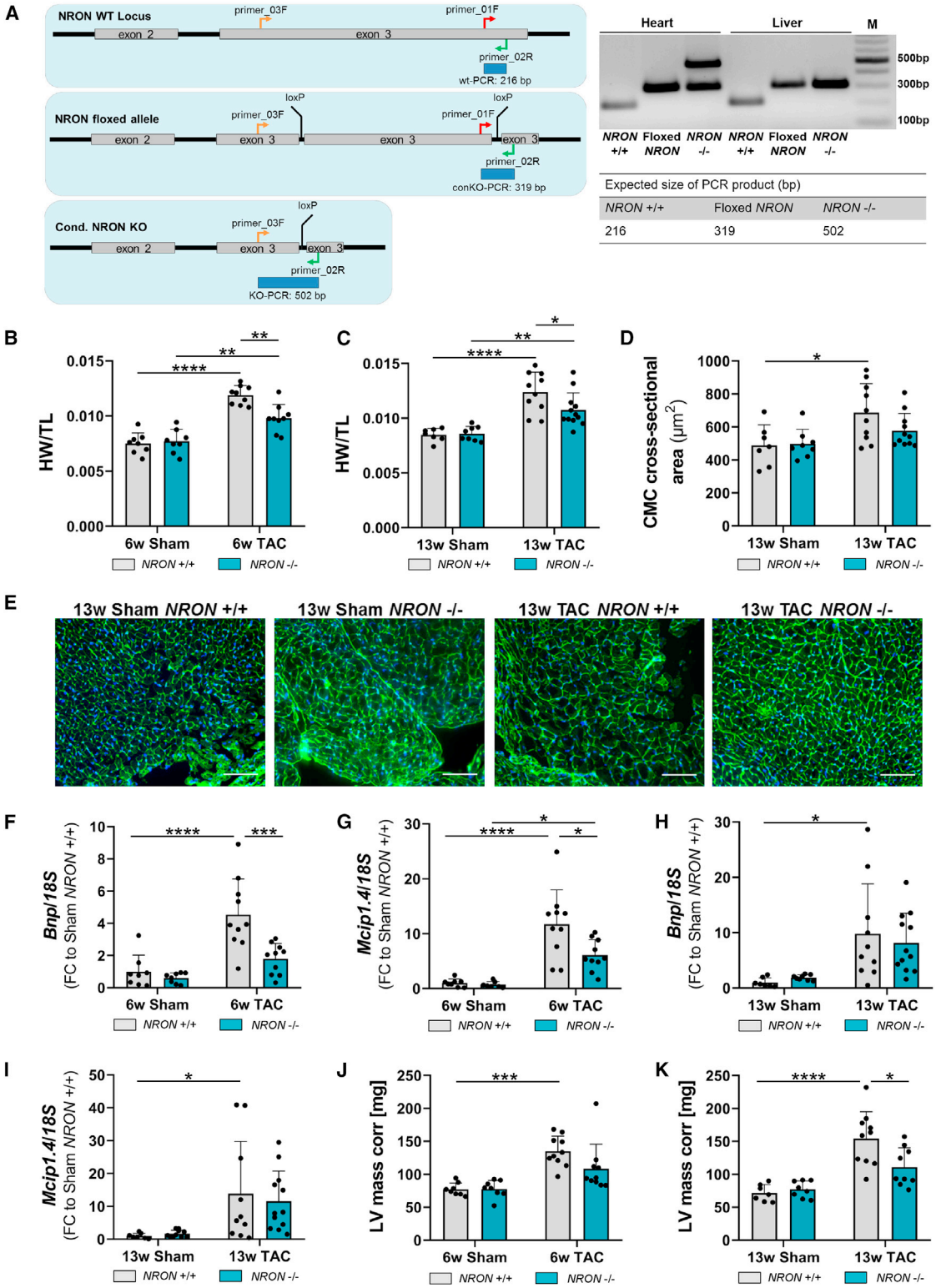

(legend on next page)

Transcriptome profiling of *NRON* KO hearts reveals anti-hypertrophic pathway enrichment

To gain insight into the molecular processes affected by *NRON* KO in cardiac hypertrophy, we performed RNA sequencing of heart samples from WT and *NRON* KO mice 6 weeks after Sham and TAC surgery. Global gene expression was compared among three groups: WT mice exposed to Sham surgery (Sham WT), WT mice exposed to TAC surgery (TAC WT), and *NRON* KO mice exposed to TAC surgery (TAC KO). Since an anti-hypertrophic effect of *NRON* KO after TAC surgery was observed in previous experiments (see above), we had a special focus on those transcripts that showed a reverse regulation between Sham WT versus TAC WT and TAC WT versus TAC KO groups. Transcripts with a significantly different abundance in the three animal groups plus the described reverse regulation were displayed in a heat map (Figure 4A). A clear difference in transcript expression was detectable when comparing Sham WT and TAC WT groups. Interestingly, the investigated transcriptome of TAC KO mice was very similar to the one of Sham WT mice, thereby underlining the anti-hypertrophic effect of *NRON* KO observed before. Further analysis of significantly different regulated transcripts using the Gene Ontology Biological Process (GOBP) analysis revealed a role of *NRON* in the cellular response to mechanical stimulus as well as in heart-and cardiac-related functions (Figure 4B). Several genes known to associate with cardiac disease (e.g., *Nppa*, *Nppb*) were among the top 100 deregulated transcripts (Figure 4C and Table S4) and confirmed the anti-hypertrophic effect of *NRON* KO. We validated these findings in RNA samples from *NRON* WT and *NRON* KO mice exposed to 6 and 13 weeks of TAC or Sham surgery and confirmed the effect by studying *Anp*, *Tgfb2*, and *Ctgf* mRNA levels (Figures 4D–4F and S2).

These data clearly indicate a role of *NRON* during the induction of or the response to pressure-overload-induced cardiac hypertrophy.

DISCUSSION

Non-coding RNAs play important roles in the regulation of physiological and pathological processes. However, the specific role of the vast majority of ncRNAs is still under investigation. First insights into the function of the lncRNA *NRON* revealed an association with immunological- and cancer-related processes as well as a biomarker role in heart disease.[15–19] Since *NRON* was described as a repressor of the hypertrophy-associated transcription factor NFAT, we hypothesized that *NRON* might interfere with the regulation of hypertrophy in the cardiac system. Hence, the aim of this study was to investigate the role of *NRON* in a cardiac hypertrophy mouse model.

Indeed, *NRON* expression was clearly downregulated during pressure-overload-induced cardiac hypertrophy and significantly enriched in cardiomyocytes. In contrast to previous studies demonstrating a cytoplasmic localization of *NRON* in T cells,[13,14] we showed a mainly chromatin-associated localization of *NRON* in cardiomyocytes. To get the first details into the mechanistic role of *NRON* in a cardiovascular setting, we studied the lncRNA in primary NMCMs. Again, a clear downregulation was visible after hypertrophic induction, while hypertrophy markers were upregulated. Surprisingly, an overexpression using AAV6 viral particles led to a pro-hypertrophic effect in NMCMs.

These findings are in stark contrast to our own hypothesis that *NRON* functions as a repressor of NFAT-mediated hypertrophy. Gain-of-function experiments *in vivo* by cardiomyocyte-specific *NRON* overexpression also revealed a pro-hypertrophic effect of *NRON* in the murine TAC model. Accordingly, loss of function by cardiomyocyte-specific *NRON* KO showed an anti-hypertrophic effect upon TAC surgery in mice. Elevated or reduced heart weight, cardiomyocyte cell size, hypertrophic marker gene expression, and LV mass were clearly apparent for the gain- and loss-of-function models, respectively. Detailed transcriptome analyses strengthened our previous findings by demonstrating similar transcriptomic profiles of hypertrophy-induced *NRON* KO mice and Sham WT mice. Cardiac-disease-related genes, which are especially associated with hypertrophy, were among the most strongly deregulated transcripts, showing a significant upregulation upon the induction of hypertrophy by TAC surgery along with a significant downregulation upon *NRON* KO. Thereby, our data suggest a novel yet undescribed role of *NRON* in cardiomyocytes.

The subcellular localization of lncRNAs and their accompanied interaction with binding partners significantly impact their function.[21] Hence, lncRNAs can function differentially in distinct cellular compartments. The lncRNA *PYCARD-AS1*, for example, was described to function as an epigenetic regulator of its target in the nucleus, whereas it functioned as a translational regulator in the cytoplasm. Both regulatory functions were mediated by an interaction with location-specific binding partners.[22] It is postulated that a nuclear localization of lncRNAs is mediated by nuclear retention elements within the lncRNA sequence.[23] However, nuclear retention of lncRNAs

Figure 3. Cardiac hypertrophy in *NRON* KO mice

Cardiac hypertrophy was analyzed after Sham or TAC surgery in $NRON^{+/+}$ (WT) and $NRON^{-/-}$ (KO) mice. (A) Cardiomyocyte-specific *NRON* KO is mediated by cross-breeding $Cre^{tg/0}$ mice with NRON-floxed mice. For genotyping the DNA from the heart and liver tissues of $NRON^{+/+}$, floxed *NRON* and $NRON^{-/-}$ mice were extracted, and a PCR was performed using primers 01_F, 02_R, and 03_F for amplification. As a marker (M), 100 bp DNA-Marker (New England Biolabs) was used. (B and C) HW after (B) 6 and (C) 13 weeks of surgery was measured relative to the length of the murine tibia (TL). (D and E) The cardiomyocyte cross-sectional area after 13 weeks of surgery was analyzed by WGA staining and is given in μm^2. Scale bar, 100 μm. (F and G) Levels of (F) *Bnp* and (G) *Mcip1.4* mRNA after 6 weeks of surgery were measured by qPCR and normalized to *18S* RNA. (H and I) Levels of (H) *Bnp* and (I) *Mcip1.4* after 13 weeks of surgery were measured by qPCR and normalized to *18S* RNA. (J and K) LV mass corr was analyzed by echocardiography after (J) 6 and (K) 13 weeks of surgery. All data are mean ± SD; n = 7–12. *$p < 0.05$; **$p < 0.01$; ***$p < 0.001$; ****$p < 0.0001$. Two-way ANOVA with Tukey's multiple comparisons test.

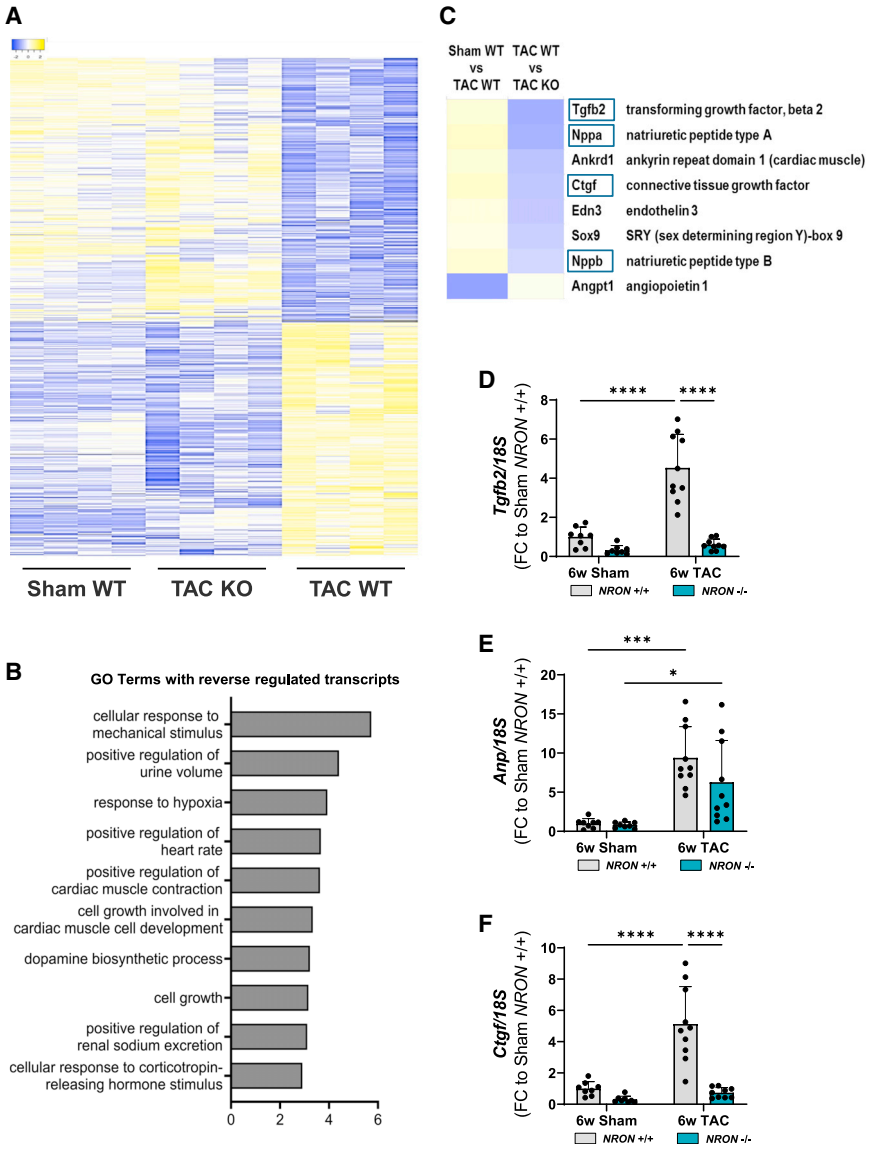

Figure 4. Transcriptomic changes upon *NRON* KO

RNA sequencing was performed in hearts from $NRON^{+/+}$ (WT) and $NRON^{-/-}$ (KO) mice after 6 weeks of Sham or TAC surgery. (A) A heat map shows significantly different mRNAs with reverse regulation between the three groups: Sham WT, TAC WT, and TAC KO. (B) Gene Ontology Biological Process (GOBP) analysis of significantly different mRNAs with reverse regulation between the three groups and a minimum FC of 1.5. n = 4; one-way ANOVA. (C) Cardiac-related genes among the top 100 deregulated mRNAs. (D–F) Levels of *Tgfb2* (D), *Anp* (E), and *Ctgf* (F) mRNA after 6 weeks of surgery were measured by qPCR and normalized to *18S* RNA. All data are mean ± SD; n = 7–12. *p < 0.05; **p < 0.01; ***p < 0.001; ****p < 0.0001. Two-way ANOVA with Tukey's multiple comparisons test.

might also depend on their interaction with binding partners that are involved in the nuclear retention process. Nuclear ribonucleoprotein K is an example of a binding partner that mediates the nuclear enrichment of its target. However, nuclear ribonucleoprotein K showed a cell-type-specific expression,[24] and, hence, subcellular localization of its target lncRNAs is cell-type-specific as well.

The lncRNA *NRON* shows a cell-type-specific localization to different subcellular compartments accompanied with a dual role in the regulation of cellular processes like hypertrophy. Therefore, the unexpected promotion of cardiac hypertrophy by *NRON* observed in this study might be a result of the differential subcellular localization of *NRON* in cardiomyocytes compared to the cytoplasmic localization in other, previously investigated cell types. Since this is the first study investigating *NRON* in cardiomyocytes, further studies need to reveal the molecular mechanisms leading to the observed pro-hypertrophic effect of *NRON* in cardiomyocytes.

MATERIALS AND METHODS

Animal procedures

Animal procedures were approved by *Niedersächsisches Landesamt für Verbraucherschutz und Lebensmittelsicherheit* (LAVES; approval number 15/1914). All animal experiments were performed in accordance with regulatory standards of the German animal protection law.

For *NRON* overexpression experiments, male C57BL/6J mice (8- to 10-weeks-old) were purchased from Charles River. WT mice (B6.129S1-Tg(Myh7-cre)1Jmk; kindly provided by Prof. Heineke, German Center for Cardiovascular Research partner site Mannheim/Heidelberg, Heidelberg, Germany) were crossbred with conditional *NRON* KO mice (C57BI/6J –$Nron^{tm2Thum}$; Ozgene, Bentley, Australia) to obtain cardiomyocyte-specific *NRON* KO mice (B6-Tg(Mhy7) 1Jmk-$NRON^{tm2Thum}$).

TAC, as a model of pressure-overload-induced cardiac hypertrophy, and Sham surgery, a similar procedure to TAC surgery but without occlusion of the aorta, were applied to 8-week-old male mice, as described previously.[25] AAV9-cTnT-*NRON* and AAV9-cTnT-empty viral particles were kindly provided by Prof. Engelhardt, Institute for Pharmacology and Toxicology, Technical University Munich, Munich, Germany. Intravenous injection of 1.5×10^{12} AAV9-*NRON* or AAV9-empty viral particles was performed at the end of the surgery process. Animals were anesthetized using 5% isoflurane in 100% O_2. Anesthesia was maintained by 1.3%–1.5% isoflurane in 100% O_2 and monitored via the toe pinch reflex. Butorphanol (2 mg/kg body weight) and Novalgin (62.5 mg/kg body weight)

were subcutaneously injected pre-surgery and 6 h post-surgery. In addition, Novalgin (200 mg/kg body weight) was provided in the drinking water for 3 days after the surgery.

Cardiac function was assessed by echocardiography (Vevo2100, Fujifilm/VisualSonics, Canada) at the indicated time points. Animals were anesthetized using 5% isoflurane in 100% O_2, and anesthesia was maintained by 0.8%–2% isoflurane in 100% O_2. Mice were sacrificed by cervical dislocation under anesthesia at the indicated endpoints, and the heart tissue was used for histological and biochemical analyses.

For TAC and Sham surgeries, animals from the same litter were taken. An AAV9 injection was done in a blinded way by the animal technician. Subsequently, echocardiography was performed in a blinded manner. Only after the analysis the data were unblinded.

Cardiac cell fractionation

Cardiomyocytes, endothelial cells, and fibroblasts were isolated from mouse hearts by retrograde perfusion.[26] Mice were anesthetized with 5% isoflurane in 100% O_2 followed by 1%–2% isoflurane in 100% O_2. Mice were injected intraperitoneally with 0.1 mL heparin (500 IU/mL), and Butorphanol (5 mg/kg body weight) was applied subcutaneously pre-surgery. Hearts were cannulated through the aorta and perfused with a pre-warmed perfusion buffer (113 mM NaCl, 4.7 mM KCl, 0.6 mM KH_2PO_4, 0.6 mM Na_2HPO_4, 1.2 mM $MgSO_4$-$7H_2O$, 0.032 mM phenol red, 12 mM $NaHCO_3$, 10 mM $KHCO_3$, 10 mM HEPES, 30 mM taurine, 0.1% glucose, 10 mM 2,3-butanedione monoxime) followed by perfusion with a pre-warmed digestion buffer (perfusion buffer supplemented with 700 U/mL collagenase II (Worthington Biochemical Cooperation, Lakewood, NJ, USA) and 12.5 μM $CaCl_2$ for 10–15 min.

The atria were removed, and ventricles were transferred into a digestion buffer and cut into small pieces. Subsequently, anesthetized animals were sacrificed by cervical dislocation.

Tissue was dissociated using a 1 mL syringe. Stop buffer (perfusion buffer containing 10% FBS and 12.5 μM $CaCl_2$) was added, and shearing was continued. A cell suspension was filtered through a 100 μm cell strainer, and a plating medium (minimum essential medium [MEM] supplemented with 10% FBS, 2 ng/mL vitamin B12, 4.2 mM NaHCO3, 100 U/mL penicillin, 100 μg/mL streptomycin) was added. Cardiomyocytes were allowed to sediment for 10 min at room temperature. A supernatant containing endothelial cells and fibroblasts was transferred to a fresh tube. Cardiomyocytes were washed with PBS, pelleted for 5 min at 3,000 rpm and 4°C, and flash-frozen in liquid nitrogen.

A cell suspension containing endothelial cells and fibroblasts was centrifuged for 5 min at 1,500 rpm and room temperature. Pelleted cells were resuspended in a plating medium, seeded into a tissue culture plate, and incubated at 37°C and 1% CO_2 for 60 min. A supernatant containing endothelial cells was transferred into a fresh tube. Endothelial cells were purified by CD146-based MACS separation (Miltenyi, Bergisch Gladbach, Germany) according to the manufacturer's protocol. Briefly, endothelial cells were pelleted for 5 min at 1,500 rpm and 4°C, resuspended in MACS buffer, and mixed with CD146 MicroBeads. After incubation for 15 min at 4°C, cells were washed with MACS buffer and centrifuged for 5 min at 1,500 rpm and 4°C. Cells were resuspended in MACS buffer and applied onto MS column. CD146-positive cells were isolated in the magnetic field, centrifuged for 5 min at 3,000 rpm and 4°C, and flash-frozen in liquid nitrogen.

Fibroblasts were detached from the tissue culture plate using a cell scraper, centrifuged for 5 min at 3,000 rpm and 4°C, and flash-frozen in liquid nitrogen.

Cell culture and subcellular fractionation

NMCMs/neonatal rat cardiomyocytes (NRCMs) were isolated from 1-to-3-day-old mouse babies using the Neonatal Heart Dissociation Kit (Miltenyi). The primary cardiomyocytes were maintained in MEM (Bioconcept) with 5% FBS (Gibco), 1% Penicillin/streptomycin (Life Technologies), 100 nM BrdU (Sigma), and 2 μg/mL vitamin B12 (Sigma).

AAV6-cTnT-*NRON* and AAV6-cTnT-empty viral particles were kindly provided by Prof. Engelhardt, Institute for Pharmacology and Toxicology, Technical University Munich, Munich, Germany. The infection of NMCMs was done using viral particles at an MOI of 5×10^3 for 72 h.

For hypertrophic treatment, NMCMs were cultured in MEM with 1% FBS (Gibco), 1% Penicillin/streptomycin (Life Technologies), 100 nM BrdU (Sigma), and 2 μg/mL vitamin B12 (Sigma) supplemented with 100 μM phenylephrine hydrochloride (Sigma) and isoprenaline hydrochloride (Sigma) for 48 h. The subcellular fractionation of NMCMs into cytoplasmic, nuclear-soluble, and chromatin-associated fractions was performed as described previously.[27] In brief, cells were dissociated by trypsin, washed with PBS, and centrifuged for 5 min at 500 × g. Pelleted cells were lysed in RLN1 buffer (50 mM Tris-HCl pH 8.0, 140 mM NaCl, 1.5 mM MgCl2, 0.5% Igepal, 2 mM Vanadyl Ribonucleosid Complex) and incubated for 5 min on ice. The lysate was centrifuged for 2 min at 300 × g and 4°C. The supernatant, which contains the cytoplasmic fraction, was transferred to a fresh tube and stored on ice. The pellet was lysed with RLN2 buffer (50 mM Tris-HCl pH 8.0, 500 mM NaCl, 1.5 mM MgCl2, 0.5% Igepal, 2 mM Vanadyl Ribonucleoside Complex) for 5 min on ice. The lysate was centrifuged for 2 min at 16,400 × g. The supernatant, which contains the nuclear-soluble fraction, and the pellet, which contains the chromatin-associated fraction, were each transferred into fresh tubes and used for RNA isolation and gene expression analyses.

RNA-FISH

NRON RNA-FISH was performed by using the ViewRNA Cell Plus Assay (Thermo Fisher Scientific, Waltham, MA, USA) in NMCM

cells. All the buffers mentioned here were provided by the kit except for the PBS. Cells were cultured in an 8-well chamber slide (Thermo Fisher Scientific, 8×10^4 cells/well) and first fixed and permeabilized with a Fixation/Permeabilization solution for 30 min at room temperature. After being washed three times with 1× PBS/RNase inhibitor, the fixed cells were first incubated with *NRON*-specific Probe Sets (1:100, type I probe, 546 nm) for 2 h at 40°C. NMCM cells were next incubated one after one with PreAmplifier Mix (1:25), Amplifier Mix (1:25), and Label Probe Mix (1:25, incubated in the dark) for 1 h at 40°C. In between the probe incubation, cells were washed with Wash Buffer Solution five times. After all four Probe Sets/Mix stainings, cells were stained with DAPI for 5–15 min at room temperature in the dark. Images were taken with the Leica SP8 confocal microscope.

Cardiomyocyte cross-sectional area measurement

Cryo sections of mouse heart tissue were fixed with 4% paraformaldehyde and permeabilized with 0.1% Triton X-100 in PBS. The sections were stained with wheat germ agglutinin (WGA) coupled with Alexa Flour 488 (1:100 in PBS; Thermo Fisher Scientific, Waltham, MA, USA) for 40 min in the dark. Nuclei were counterstained with 5 μg/mL Dapi (Sigma-Aldrich, St. Louis, MO, USA). Images were acquired with a Nikon Eclipse Ti-U microscope (Nikon, Melville, NY, USA) and NIS-Elements BR 3.2 software (Nikon Instruments, Tokyo, Japan).

RNA isolation and gene expression analysis

Total RNA was isolated using the TriFast method (VWR, Darmstadt, Germany) according to the manufacturer's protocol. RNA was quantified using Synergy HT Bioreader (Biotek, Winooski, VT, USA). Isolated RNA (100–500 ng, according to sample concentration) was reverse-transcribed using the iScript Select cDNA Synthesis Kit (Bio-Rad, Hercules, CA, USA). For the quantification of gene expression, gene-specific primer sets (Table S5) and the iQ Sybr Green Mastermix were used. Gene expression was measured by ViiA7 (Thermo Fisher Scientific, Waltham, MA, USA) or the CFX384 Touch (BioRad, Hercules, CA, USA) real-time PCR detection system.

Absolute mRNA quantification

The copy number of *NRON* was quantified by qPCR and a plasmid standard curve, as described previously.[28]

PCR for genotyping

For the genotyping of mouse samples, genomic DNA was isolated using the DNeasy Blood & Tissue Kit (Qiagen, Hilden, Germany) performing RNAse A digest according to the manufacturer's instructions. For the amplification of specific DNA fragments, PCR was performed with the reverse and forward primers for the specific gene product using the HotStarTaq Master Mix Kit (Qiagen) and 200 ng gDNA. The cycling conditions were 94°C for 3 min, 35 cycles of 94°C for 30 s, 65°C for 30 s, 72°C for 50 s, the final elongation at 72°C for 5 min, and hold at 4°C. For visualization, we performed gel electrophoresis using a 2% agarose gel. We used the 100 bp DNA-Marker (New England Biolabs, Ipswich, Massachusetts, USA) as a reference.

Transcriptome profiling

Total RNA was isolated from mouse hearts after 6 weeks of TAC or Sham surgery using the MiRNeasy Kit (Qiagen, Hilden, Germany) in four biological replicates per group. RNA quantity and quality were analyzed by Agilent Bioanalyzer and the RNA 6000 Nano Kit (Agilent Technologies, Santa Clara, CA, USA). Subsequent mRNA sequencing (NextSeq 550, 1 × 75 bp) was performed at the Research Core Unit Transcriptomics of Hannover Medical School (Hannover, Germany). 250 ng of total RNA per sample were utilized as input for the mRNA enrichment procedure with "NEBNext Poly(A) mRNA Magnetic Isolation Module" (E7490L; New England Biolabs) followed by stranded cDNA library generation using "NEBNext Ultra II Directional RNA Library Prep Kit for Illumina" (E7760L; New England Biolabs). Raw reads were aligned to the mouse genome (GRCm38 release M18) using STAR,[29] and quantification of the mapped reads was performed with featureCounts.[30] Deseq2[31] was then used for read counts normalization and differential expression analysis. RNA sequencing (RNA-seq) data have been deposited in the GEO database (GEO: GSE188762).

Statistics

Statistical analyses were performed using Graph Pad Prism software. Unpaired two-tailed Student's t-test, one-way ANOVA with Sidak multiple comparisons test, and two-way ANOVA with Tukey's multiple comparisons test were applied as appropriate and as indicated in the figure legends. Data are shown as mean ± SD of biologically independent experiments. Differences were considered statistically significant at p values below 0.05 and are marked with asterisks (*$p < 0.05$, **$p < 0.01$, ***$p < 0.001$, ****$p < 0.0001$).

SUPPLEMENTAL INFORMATION

Supplemental information can be found online at https://doi.org/10.1016/j.ymthe.2021.11.018.

ACKNOWLEDGMENTS

We acknowledge the support of the Core Facility for Genomics (RCUG) at Hannover Medical School. We acknowledge the support of the Research Core Unit for Laser Microscopy at Hannover Medical School. We thank Jörg Heineke for providing Myh7-cre mice. We thank H. Janssen-Peters for supporting animal experiments. We thank K. Zimmer, K. Scherf, A. Gietz, N. Ernst, A. Korte, I. Riedel, and J. Bode for technical support. This study was funded by the Deutsche Forschungsgemeinschaft (RE 3523/1-1 | TH 903/11-1 given to K.R. and T.T.) and SFB/Transregio (TRR267 to S.E., C.B., and T.T.).

AUTHOR CONTRIBUTIONS

J.H. and J.L. designed research studies, conducted the majority of experiments, acquired and analyzed data, and wrote the manuscript. D.L, K.S., S.B., and H.J.H. acquired data. A.F. conducted echocardiography experiments and acquired and analyzed data. K.X. analyzed RNA-seq data. K.R. designed research studies. D.R. and S.E. provided

AAV9 and AAV6 viral particles. C.B. and T.T. designed research studies and revised the manuscript.

DECLARATION OF INTERESTS

T.T. and C.B. filed patents in the field of ncRNAs. T.T. is founder and holds shares of Cardior Pharmaceuticals GmbH. All other authors declare no competing interests.

REFERENCES

1. Mattick, J.S., and Rinn, J.L. (2015). Discovery and annotation of long noncoding RNAs. Nat. Struct. Mol. Biol. *22*, 5–7.
2. Hobuß, L., Bär, C., and Thum, T. (2019). Long non-coding RNAs: at the heart of cardiac dysfunction? Front Physiol. *10*, 30.
3. Klattenhoff, C.A., Scheuermann, J.C., Surface, L.E., Bradley, R.K., Fields, P.A., Steinhauser, M.L., Ding, H., Butty, V.L., Torrey, L., Haas, S., et al. (2013). Braveheart, a long noncoding RNA required for cardiovascular lineage commitment. Cell *152*, 570–583.
4. Grote, P., Wittler, L., Hendrix, D., Koch, F., Währisch, S., Beisaw, A., Macura, K., Bläss, G., Kellis, M., Werber, M., et al. (2013). The tissue-specific lncRNA Fendrr is an essential regulator of heart and body wall development in the mouse. Dev. Cell *24*, 206–214.
5. Piccoli, M.T., Gupta, S.K., Viereck, J., Foinquinos, A., Samolovac, S., Kramer, F.L., Garg, A., Remke, J., Zimmer, K., Batkai, S., et al. (2017). Inhibition of the cardiac fibroblast-enriched lncRNA Meg3 prevents cardiac fibrosis and diastolic dysfunction. Circ. Res. *121*, 575–583.
6. Viereck, J., Kumarswamy, R., Foinquinos, A., Xiao, K., Avramopoulos, P., Kunz, M., Dittrich, M., Maetzig, T., Zimmer, K., Remke, J., et al. (2016). Long noncoding RNA Chast promotes cardiac remodeling. Sci. Transl Med. *8*, 326ra22.
7. Viereck, J., Bührke, A., Foinquinos, A., Chatterjee, S., Kleeberger, J.A., Xiao, K., Janssen-Peters, H., Batkai, S., Ramanujam, D., Kraft, T., et al. (2020). Targeting muscle-enriched long non-coding RNA H19 reverses pathological cardiac hypertrophy. Eur. Heart J. *41*, 3462–3474.
8. Chatterjee, S., Bär, C., and Thum, T. (2017). Linc-ing the noncoding genome to heart function: beating hypertrophy. Trends Mol. Med. *23*, 577–579.
9. Bär, C., Chatterjee, S., and Thum, T. (2016). Long noncoding RNAs in cardiovascular pathology, diagnosis, and therapy. Circulation *134*, 1484–1499.
10. Wilkins, B.J., Dai, Y.S., Bueno, O.F., Parsons, S.A., Xu, J., Plank, D.M., Jones, F., Kimball, T.R., and Molkentin, J.D. (2004). Calcineurin/NFAT coupling participates in pathological, but not physiological, cardiac hypertrophy. Circ. Res. *94*, 110–118.
11. Wilkins, B.J., and Molkentin, J.D. (2004). Calcium-calcineurin signaling in the regulation of cardiac hypertrophy. Biochem. Biophys. Res. Commun. *322*, 1178–1191.
12. Dirkx, E., da Costa Martins, P.A., and De Windt, L.J. (2013). Regulation of fetal gene expression in heart failure. Biochim. Biophys. Acta *1832*, 2414–2424.
13. Willingham, A.T., Orth, A.P., Batalov, S., Peters, E.C., Wen, B.G., Aza-Blanc, P., Hogenesch, J.B., and Schultz, P.G. (2005). A strategy for probing the function of noncoding RNAs finds a repressor of NFAT. Science *309*, 1570–1573.
14. Sharma, S., Findlay, G.M., Bandukwala, H.S., Oberdoerffer, S., Baust, B., Li, Z., Schmidt, V., Hogan, P.G., Sacks, D.B., and Rao, A. (2011). Dephosphorylation of the nuclear factor of activated T cells (NFAT) transcription factor is regulated by an RNA-protein scaffold complex. Proc. Natl. Acad. Sci. U S A *108*, 11381–11386.
15. Imam, H., Bano, A.S., Patel, P., Holla, P., and Jameel, S. (2015). The lncRNA NRON modulates HIV-1 replication in a NFAT-dependent manner and is differentially regulated by early and late viral proteins. Sci. Rep. *5*, 8639.
16. Li, J., Chen, C., Ma, X., Geng, G., Liu, B., Zhang, Y., Zhang, S., Zhong, F., Liu, C., Yin, Y., et al. (2016). Long noncoding RNA NRON contributes to HIV-1 latency by specifically inducing tat protein degradation. Nat. Commun. *7*, 11730.
17. Yao, Z., Xiong, Z., Li, R., Liang, H., Jia, C., and Deng, M. (2018). Long non-coding RNA NRON is downregulated in HCC and suppresses tumour cell proliferation and metastasis. Biomed. Pharmacother. *104*, 102–119.
18. Niu, L., Fan, Q., Yan, M., and Wang, L. (2019). LncRNA NRON down-regulates lncRNA snaR and inhibits cancer cell proliferation in TNBC. Biosci. Rep. *39*, BSR20190468.
19. Xuan, L., Sun, L., Zhang, Y., Huang, Y., Hou, Y., Li, Q., Guo, Y., Feng, B., Cui, L., Wang, X., et al. (2017). Circulating long non-coding RNAs NRON and MHRT as novel predictive biomarkers of heart failure. J. Cell Mol Med *21*, 1803–1814.
20. Wang, Y., Xu, P., Zhang, C., Feng, J., Gong, W., Ge, S., and Guo, Z. (2019). LncRNA NRON alleviates atrial fibrosis via promoting NFATc3 phosphorylation. Mol. Cell Biochem *457*, 169–177.
21. Bridges, M.C., Daulagala, A.C., and Kourtidis, A. (2021). LNCcation: lncRNA localization and function. J. Cell Biol *220*, e202009045.
22. Miao, H., Wang, L., Zhan, H., Dai, J., Chang, Y., Wu, F., Liu, T., Liu, Z., Gao, C., Li, L., et al. (2019). A long noncoding RNA distributed in both nucleus and cytoplasm operates in the PYCARD-regulated apoptosis by coordinating the epigenetic and translational regulation. Plos Genet. *15*, e1008144.
23. Palazzo, A.F., and Lee, E.S. (2018). Sequence determinants for nuclear retention and cytoplasmic export of mRNAs and lncRNAs. Front Genet. *9*, 440.
24. Lubelsky, Y., and Ulitsky, I. (2018). Sequences enriched in Alu repeats drive nuclear localization of long RNAs in human cells. Nature *555*, 107–111.
25. Rockman, H.A., Ross, R.S., Harris, A.N., Knowlton, K.U., Steinhelper, M.E., Field, L.J., Ross, J., Jr., and Chien, K.R. (1991). Segregation of atrial-specific and inducible expression of an atrial natriuretic factor transgene in an in vivo murine model of cardiac hypertrophy. Proc. Natl. Acad. Sci. U S A *88*, 8277–8281.
26. O'Connell, T.D., Rodrigo, M.C., and Simpson, P.C. (2007). Isolation and culture of adult mouse cardiac myocytes. Methods Mol. Biol. *357*, 271–296.
27. Cabianca, D.S., Casa, V., Bodega, B., Xynos, A., Ginelli, E., Tanaka, Y., and Gabellini, D. (2012). A long ncRNA links copy number variation to a polycomb/trithorax epigenetic switch in FSHD muscular dystrophy. Cell *149*, 819–831.
28. Feretzaki, M., Nunes, P.R., and Lingner, J. (2019). Expression and differential regulation of human TERRA at several chromosome ends. RNA *25*, 1470–1480.
29. Dobin, A., Davis, C.A., Schlesinger, F., Drenkow, J., Zaleski, C., Jha, S., Batut, P., Chaisson, M., and Gingeras, T.R. (2013). STAR: ultrafast universal RNA-seq aligner. Bioinformatics *29*, 15–21.
30. Liao, Y., Smyth, G.K., and Shi, W. (2014). featureCounts: an efficient general purpose program for assigning sequence reads to genomic features. Bioinformatics *30*, 923–930.
31. Love, M.I., Huber, W., and Anders, S. (2014). Moderated estimation of fold change and dispersion for RNA-seq data with DESeq2. Genome Biol. *15*, 550.

YMTHE, Volume *30*

Supplemental Information

The long non-coding RNA *NRON* promotes the development of cardiac hypertrophy in the murine heart

Jeannine Hoepfner, Julia Leonardy, Dongchao Lu, Kevin Schmidt, Hannah J. Hunkler, Sinje Biß, Ariana Foinquinos, Ke Xiao, Kumarswamy Regalla, Deepak Ramanujam, Stefan Engelhardt, Christian Bär, and Thomas Thum

Figure S1

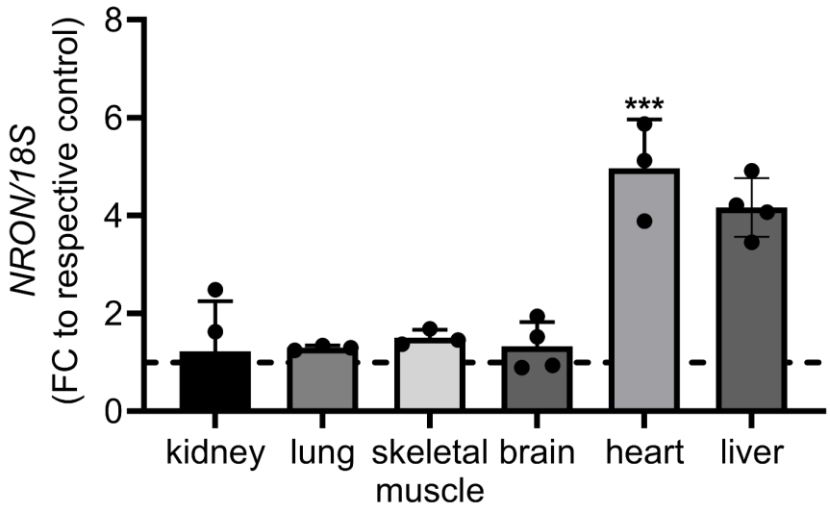

Figure S1: *NRON* level in different organs after AAV9-*NRON* administration. 1.5x10^{12} AAV9-*NRON* or AAV9-empty viral particles were injected. Mice were sacrificed after 6 weeks. *NRON* level was measured by qPCR relative to *18S* RNA. FC was calculated using *NRON* level in the respective AAV9-empty injected organ as control. All data are mean ± S.D.; n=3-4. *P<0.05; **P<0.01; ***P<0.001; ****P<0.0001; Student's t-test.

Table S1: Ct values of samples from figure 1 and 2. (100-500 ng RNA was used for cDNA synthesis according to the concentration of the sample).

Experiment	Sample	Ct value NRON	Ct value Housekeeper
Figure 1a	chromatin associated	27.89	
	cytoplasmic fraction	31.5	
	Nuclear soluble	33	
Figure 1b	CMC	29,46	21,93
	CF	30,65	21,56
	EC	32,13	22,22
Figure 1c	2w Sham	24,155	22,06
	2w TAC	25,17	21,44
	4w Sham	29,65	21,31
	4w TAC	29,73	21,45
	6w Sham	29,79	21,41
	6w TAC	29,95	21,37
	8w Sham	27,79	20,95
	8w TAC	28	20,84
	13w Sham	30,16	22,13
	13w TAC	30,15	21,07
Figure 2a	AAV9-Empty	29,02	10,75
	AAV9-*NRON*	27,11	11,01

Table S2: Echocardiography analysis after TAC surgery in AAV9-*NRON* injected mice.

	Sham AAV9-empty	Sham AAV9-*NRON*	TAC AAV9-empty	TAC AAV9-*NRON*
Ejection fraction [%]	80.87 ± 8.66	72.3 ± 10.96	69.89 ± 13.79	64.85 ± 18.24
Fractional shortening [%]	49.56 ± 9.36	41.64 ± 8.66	39.84 ± 11.09	36.29 ± 12.3
LV mass [mg]	138.3 ± 37.86	136.9 ± 13.26	165.2 ± 38.39	184 ± 33.14
LV mass corr [mg]	110.6 ± 30.29	109.5 ± 10.61	132.2 ± 30.72	147.2 ± 26.51
IVS;d [mm]	1.2 ± 0.12	1.16 ± 0.12	1.34 ± 0.26	1.2 ± 0.17
IVS;s [mm]	1.79 ± 0.19	1.51 ± 0.17	1.7 ± 0.34	1.64 ± 0.21
LVID;d [mm]	3.53 ± 0.29	3.8 ± 0.29	3.48 ± 0.3	3.75 ± 0.52
LVID;s [mm]	1.76 ± 0.37	2.21 ± 0.53	2.08 ± 0.52	2.38 ± 0.79
LVPW;d [mm]	0.86 ± 0.3	0.79 ± 0.16	1.06 ± 0.26	1.16 ± 0.23
LVPW;s [mm]	1.27 ± 0.33	1.12 ± 0.31	1.42 ± 0.31	1.53 ± 0.37
diameter;s [mm]	1.76 ± 0.4	2.25 ± 0.51	2.09 ± 0.5	2.14 ± 0.28
diameter;d [mm]	3.48 ± 0.25	3.82 ± 0.23	3.44 ± 0.29	3.72 ± 0.5
volume;s [uL]	9.96 ± 5.52	18.53 ± 10.75	15.55 ± 8.52	15.62 ± 5.25
volume;d [uL]	50.69 ± 8.65	63.06 ± 8.92	49.39 ± 9.41	53.17 ± 7.07

Echocardiography parameters are displayed as mean ± SD. LV mass, left ventricular mass; LV mass corr, left ventricular mass corrected; IVS;d, intraventricular septum thickness in diastole; IVS;s, intraventricular septum thickness in systole ; LVID;d, left ventricular internal diameter in diastole; LVID;s, left ventricular internal diameter in systole; LVPW;d, left ventricular posterior wall thickness in diastole; LVPW;s, left ventricular posterior wall thickness in systole; diameter;s, systolic diameter; diamter;d, diastolic diameter; volume;s, systolic volume; volume;d, diastolic volume.

Table S3: Echocardiography analysis after TAC surgery in *NRON*-KO mice.

	2w Sham *NRON* +/+	2w Sham *NRON* -/-	2w TAC *NRON* +/+	2w TAC *NRON* -/-
Ejection fraction [%]	53.97 ± 8.96	62.46 ± 14.63	49.3 ± 9.43	65.38 ± 9.88
Fractional shortening [%]	27.63 ± 5.54	34.27 ±- 10.7	24.92 ± 6.15	35.77 ± 7.46
LV mass [mg]	95.21 ± 15.88	105.5 ± 22.31	133.6 ± 28.02	115.1 ± 23.62
LV mass corr [mg]	76.17 ± 12.7	84.4 ± 17.85	106.8 ± 22.41	92.05 ± 18.89
IVS;d [mm]	0.79 ± 0.17	0.76 ± 0.08	0.93 ± 0.11	0.9 ± 0.13
IVS;s [mm]	0.98 ± 0.21	0.96 ± 0.13	1.14 ± 0.15	1.07 ± 0.14
LVID;d [mm]	3.72 ± 0.38	3.88 v 0.38	4.04 ± 0.36	3.69 v 0.28
LVID;s [mm]	2.7 ± 0.41	2.61 v 0.61	3.04 ± 0.41	2.39 ± 0.41
LVPW;d [mm]	0.75 ± 0.21	0.79 ± 0.13	0.81 ± 0.14	0.82 ± 0.06
LVPW;s [mm]	0.87 ± 0.18	0.96 ± 0.1	0.99 ± 0.14	1.12 ± 0.15
diameter;s [mm]	2.71 ± 0.41	2.57 ± 0.59	3.07 ± 0.42	2.38 ± 0.42
diameter;d [mm]	3.74 ± 0.34	3.87 ± 0.38	4.08 ± 0.36	3.68 ± 0.29
volume;s [uL]	28.38 ± 10.44	25.76 ± 13.74	38.23 ± 11.69	20.75 ± 8.46
volume;d [uL]	60.22 ± 12.7	65.58 ± 15.5	74.37 ± 15.6	57.96 ± 10.56
	6w Sham *NRON* +/+	**6w Sham *NRON* -/-**	**6w TAC *NRON* +/+**	**6w TAC *NRON* -/-**
Ejection fraction [%]	52.04 ± 11.47	65.83 ± 6.01	42.54 ± 9.46	59.29 ± 8.93
Fractional shortening [%]	26.72 ± 7.34	35.93 ± 4.59	21.03 ± 5.44	31.24 ± 6.13
LV mass [mg]	96.6 ± 11.9	97.31 ± 16.22	168.6 ± 28.69	121.9 ± 17.14
LV mass corr [mg]	77.28 ± 9.52	77.84 ± 12.98	134.9 ± 22.95	97.55 ± 13.71
IVS;d [mm]	0.75 ± 0.1	0.81 ± 0.13	1.04 ± 0.09	1 ± 0.15
IVS;s [mm]	0.89 ± 0.13	0.99 ± 0.09	1.21 ± 0.14	1.11 ±- 0.26
LVID;d [mm]	4.05 v 0.37	3.89 ± 0.32	4.38 ± 0.24	3.76 ± 0.36
LVID;s [mm]	3 ± 0.57	2.5 ± 0.22	3.48 ± 0.3	2.61 ± 0.42
LVPW;d [mm]	0.64 ± 0.08	0.61 ± 0.1	0.86 ± 0.25	0.89 ± 0.2
LVPW;s [mm]	0.87 ± 0.15	0.86 ± 0.15	0.99 ± 0.23	1.09 ± 0.21
diameter;s [mm]	3.01 ± 0.54	2.5 ± 0.22	3.52 ± 0.31	2.61 ± 0.43
diameter;d [mm]	4.08 v 0.37	3.9 ± 0.32	4.45 ± 0.23	3.77 ± 0.37
volume;s [uL]	36.93 ± 15.28	22.55 ± 4.8	52.05 ± 11.16	25.79 ± 10.46
volume;d [uL]	74.17 ± 15.86	66.63 ± 12.76	90.41 ± 10.54	61.73 ± 14.83
	13w Sham *NRON* +/+	**13w Sham *NRON* -/-**	**13w TAC *NRON* +/+**	**13w TAC *NRON* -/-**
Ejection fraction [%]	64.24 ± 7.56	60.43 ± 4.95	39.95 ± 7.97	44.05 ± 5.48
Fractional shortening [%]	34.92 ± 5.4	32 ± 3.48	19.54 ± 4.47	21.66 ± 3.16
LV mass [mg]	89.58 ± 15.97	96.69 ± 15.81	192.5 ± 51.47	138.7 ± 36.69
LV mass corr [mg]	71.66 ± 12.78	77.35 ± 12.65	154 ± 41.18	111 ± 29.36
IVS;d [mm]	0.71 ± 0.07	0.74 ± 0.12	0.96 ± 0.16	0.9 ± 0.16
IVS;s [mm]	0.93 ± 0.08	0.82 ± 0.07	1.13 ± 0.08	1.01 ± 0.19
LVID;d [mm]	4.14 ± 0.34	3.99 ± 0.3	4.71 ± 0.46	4.14 ± 0.48
LVID;s [mm]	2.72 ± 0.45	2.77 ± 0.17	3.8 ± 0.54	3.2 ± 0.43
LVPW;d [mm]	0.6 ± 0.09	0.6 ± 0.06	0.95 ± 0.15	0.88 ± 0.18
LVPW;s [mm]	0.88 ± 0.09	0.81 ± 0.11	1.05 ± 0.15	0.94 ± 0.27
diameter;s [mm]	2.7 v 0.42	2.79 ± 0.18	3.76 ± 0.5	3.3 ± 0.38
diameter;d [mm]	4.13 ± 0.32	4.1 v 0.2	4.66 ± 0.44	4.22 ± 0.45
volume;s [uL]	28.1 ± 10.94	29.46 ± 4.58	61.83 ± 19.8	45.11 ± 13.16
volume;d [uL]	76.37 ± 13.88	74.56 ± 8.68	101.5 ± 22.99	80.44 ± 20.9

Table S3:

Echocardiography parameters are displayed as mean ± SD. LV mass, left ventricular mass; LV mass corr, left ventricular mass corrected; IVS;d, intraventricular septum thickness in diastole; IVS;s, intraventricular septum thickness in systole ; LVID;d, left ventricular internal diameter in diastole; LVID;s, left ventricular internal diameter in systole; LVPW;d, left ventricular posterior wall thickness in diastole; LVPW;s, left ventricular posterior wall thickness in systole; diameter;s, systolic diameter; diamter;d, diastolic diameter; volume;s, systolic volume; volume;d, diastolic volume.

Table S4: Top 100 deregulated mRNAs.

		Sham WT vs TAC WT		TAC WT vs TAC KO	
Gene name	**Gene description**	**fold change**	**p-value**	**fold change**	**p-value**
Gm4544	predicted gene 4544	-1.75	1.74E-14	1.72	1.75E-14
Tgfb2	transforming growth factor, beta 2	1.97	8.12E-39	-1.61	6.70E-23
Nppa	natriuretic peptide type A	2.62	1.04E-40	-1.56	6.84E-31
Ppm1e	protein phosphatase 1E (PP2C domain containing)	1.55	1.76E-32	-1.57	3.84E-30
Syndig1	synapse differentiation inducing 1	2.64	5.05E-27	-1.55	5.56E-11
Scd4	stearoyl-coenzyme A desaturase 4	-1.51	9.55E-12	1.44	2.35E-09
Aldob	aldolase B, fructose-bisphosphate	-1.87	6.34E-14	1.42	1.50E-09
Dok5	docking protein 5	1.36	2.34E-11	-1.32	8.89E-10
Acot1	acyl-CoA thioesterase 1	-1.38	2.23E-17	1.31	2.04E-14
Gm13054	predicted gene 13054	2.36	2.28E-27	-1.26	1.09E-08
Ankrd1	ankyrin repeat domain 1 (cardiac muscle)	2.04	2.12E-23	-1.24	3.15E-15
Lad1	ladinin	-1.23	4.08E-10	1.24	8.93E-10
Gm40841	predicted gene, 40841	-1.94	1.50E-15	1.21	6.43E-07
Lgi1	leucine-rich repeat LGI family, member 1	-1.23	7.04E-12	1.21	1.04E-11
Nuak1	NUAK family, SNF1-like kinase, 1	1.45	1.58E-41	-1.20	2.85E-17
Mybl1	myeloblastosis oncogene-like 1	1.18	1.07E-10	-1.23	1.73E-11
Apold1	apolipoprotein L domain containing 1	1.20	5.70E-16	-1.18	3.31E-14
Frat1	frequently rearranged in advanced T cell lymphomas	-1.38	1.74E-10	1.18	8.46E-08
Lrrc4b	leucine rich repeat containing 4B	-1.18	7.02E-18	1.19	7.75E-14
Gm24474	predicted gene, 24474	-1.19	3.21E-08	1.18	4.30E-08
Gm19277	predicted gene, 19277	-1.41	1.01E-08	1.17	1.68E-06
Ctgf	connective tissue growth factor	2.50	1.60E-78	-1.14	3.47E-07
Gm29773	predicted gene, 29773	3.23	4.70E-42	-1.13	8.56E-07
Gpr3	G-protein coupled receptor 3	1.21	1.86E-06	-1.13	2.04E-06
Grip1	glutamate receptor interacting protein 1	1.49	1.39E-09	-1.11	1.43E-06
Angpt1	angiopoietin 1	-1.91	6.35E-35	1.11	5.61E-12
Slc22a4	solute carrier family 22 (organic cation transporter), member 4	1.51	3.57E-49	-1.11	4.88E-21
Edn3	endothelin 3	1.74	3.79E-23	-1.10	2.56E-09
Hmgcs2	3-hydroxy-3-methylglutaryl-Coenzyme A synthase 2	-1.09	1.30E-05	1.22	7.54E-09
AC165271.1	novel transcript, antisense to Kcnj6	2.08	1.03E-24	-1.09	2.64E-08
Tg	thyroglobulin	-1.09	5.54E-07	1.32	2.15E-10
Hspa1a	heat shock protein 1A	1.84	3.10E-13	-1.07	1.25E-05
Pou3f1	POU domain, class 3, transcription factor 1	1.34	7.97E-09	-1.06	3.63E-06
Wnk4	WNK lysine deficient protein kinase 4	-1.06	6.04E-12	1.13	1.08E-11
Hsp90aa1	heat shock protein 90, alpha (cytosolic), class A member 1	1.06	1.47E-23	-1.06	4.39E-15
A730036I17Rik	RIKEN cDNA A730036I17 gene	1.70	2.50E-12	-1.05	2.96E-06
Hbegf	heparin-binding EGF-like growth factor	1.75	1.28E-30	-1.05	1.68E-06
2310039L15Rik	RIKEN cDNA 2310039L15 gene	-1.03	1.11E-10	1.30	1.13E-17
Uckl1os	uridine-cytidine kinase 1-like 1, opposite strand	-1.61	5.41E-15	1.03	2.19E-05
Nmrk2	nicotinamide riboside kinase 2	1.69	3.03E-11	-1.02	3.05E-05
Tent5a	terminal nucleotidyltransferase 5A	1.09	1.41E-20	-1.01	1.27E-14
Shisa6	shisa family member 6	-1.01	9.54E-06	1.10	7.58E-07
Fbp2	fructose bisphosphatase 2	-1.03	1.47E-12	1.01	2.70E-10
Synpo2l	synaptopodin 2-like	1.70	3.38E-17	-1.00	1.71E-06
Shisa3	shisa family member 3	1.00	4.67E-07	-1.07	1.15E-06
Gal3st3	galactose-3-O-sulfotransferase 3	-1.35	1.51E-29	0.99	2.38E-09
Clec18a	C-type lectin domain family 18, member A	-1.37	8.92E-09	0.99	2.19E-05
Sox9	SRY (sex determining region Y)-box 9	1.41	4.79E-23	-0.98	5.43E-10
Serpinb1c	serine (or cysteine) peptidase inhibitor, clade B, member 1c	3.11	7.13E-52	-0.98	4.77E-05
Ripor2	RHO family interacting cell polarization regulator 2	-0.97	1.87E-11	1.12	1.15E-11
Nr4a3	nuclear receptor subfamily 4, group A, member 3	1.38	1.67E-18	-0.97	2.19E-08
Resf1	retroelement silencing factor 1	1.38	1.33E-35	-0.97	3.18E-08
Enah	ENAH actin regulator	1.44	7.61E-55	-0.97	1.24E-14
Gm10635	predicted gene 10635	-1.75	6.89E-16	0.96	2.20E-05
Car9	carbonic anhydrase 9	1.21	1.79E-06	-0.96	8.16E-05
Clcn1	chloride channel, voltage-sensitive 1	-1.68	1.41E-32	0.96	7.23E-10
Xirp2	xin actin-binding repeat containing 2	1.75	1.97E-40	-0.95	1.55E-09

Table S4

Efnb3	ephrin B3	-1.13	7.32E-18	0.95	4.56E-14
Adcy8	adenylate cyclase 8	-0.95	5.46E-05	0.95	4.18E-05
Abra	actin-binding Rho activating protein	2.10	6.29E-52	-0.95	2.17E-05
Klhl33	kelch-like 33	-1.69	1.08E-31	0.95	7.74E-08
Mrgprh	MAS-related GPR, member H	-1.41	3.44E-17	0.94	3.08E-06
Hsbp1l1	heat shock factor binding protein 1-like 1	-0.93	5.77E-06	0.96	1.48E-06
Nr4a1	nuclear receptor subfamily 4, group A, member 1	0.93	1.20E-04	-0.98	3.19E-06
Gm45457	predicted gene 45457	0.93	2.01E-06	-1.34	2.96E-13
Gm43660	predicted gene 43660	1.15	7.64E-15	-0.93	2.40E-06
Otud1	OTU domain containing 1	1.21	1.25E-09	-0.92	9.88E-05
Acta1	actin, alpha 1, skeletal muscle	3.02	2.76E-45	-0.92	3.57E-10
Gm11992	predicted gene 11992	-0.92	2.90E-04	1.27	1.72E-07
Efemp1	epidermal growth factor-containing fibulin-like extracellular matrix protein 1	-1.11	4.51E-10	0.92	1.14E-07
2310016G11Rik	RIKEN cDNA 2310016G11 gene	-1.27	2.72E-07	0.91	1.65E-04
Ucp3	uncoupling protein 3 (mitochondrial, proton carrier)	-0.90	2.06E-04	1.28	7.57E-14
Gcnt1	glucosaminyl (N-acetyl) transferase 1, core 2	1.10	2.42E-15	-0.89	1.23E-10
Xirp1	xin actin-binding repeat containing 1	1.38	4.10E-54	-0.89	7.72E-11
P3h2	prolyl 3-hydroxylase 2	1.28	2.90E-16	-0.89	1.94E-08
Alox5	arachidonate 5-lipoxygenase	-0.89	2.83E-07	0.96	8.92E-10
Lman1l	lectin, mannose-binding 1 like	2.75	4.36E-73	-0.89	1.13E-06
Cabcoco1	ciliary associated calcium binding coiled-coil 1	-1.00	1.17E-11	0.89	6.25E-09
Cadm4	cell adhesion molecule 4	-0.89	2.06E-16	1.16	1.73E-23
Gm8113	predicted gene 8113	-1.16	1.13E-06	0.88	2.14E-04
Tnnt3	troponin T3, skeletal, fast	1.01	7.14E-05	-0.88	2.95E-04
Gm36569	predicted gene, 36569	1.07	2.80E-06	-0.88	1.98E-04
Etv4	ets variant 4	1.31	2.08E-08	-0.88	7.25E-05
Fam198b	family with sequence similarity 198, member B	0.88	2.18E-15	-1.05	2.53E-19
Gdf15	growth differentiation factor 15	2.30	1.76E-21	-0.88	2.61E-04
Gpr22	G protein-coupled receptor 22	-1.76	4.38E-29	0.88	9.30E-07
Hspa1b	heat shock protein 1B	1.83	3.55E-14	-0.87	3.47E-04
Klhl38	kelch-like 38	-0.87	3.66E-04	1.24	4.07E-08
Cplx3	complexin 3	1.42	1.09E-08	-0.87	3.36E-04
Cngb3	cyclic nucleotide gated channel beta 3	-0.87	2.12E-04	1.33	5.73E-09
Gm11382	predicted pseudogene 11382	1.53	1.85E-09	-0.86	2.97E-04
P4ha1	procollagen-proline, 2-oxoglutarate 4-dioxygenase (proline 4-hydroxylase), alpha 1 polypeptide	0.86	5.14E-18	-0.95	2.80E-17
Gm31663	predicted gene, 31663	-0.86	2.89E-06	1.02	1.75E-08
Stc1	stanniocalcin 1	0.88	7.35E-09	-0.86	1.21E-06
Bcl2	B cell leukemia/lymphoma 2	0.86	3.51E-14	-1.07	6.39E-25
Kcnv2	potassium channel, subfamily V, member 2	-0.96	5.19E-05	0.85	2.76E-05
Retnla	resistin like alpha	-1.38	2.91E-09	0.85	2.65E-04
Nppb	natriuretic peptide type B	2.15	1.55E-27	-0.85	7.54E-05
Hspa1l	heat shock protein 1-like	1.36	1.15E-38	-0.85	1.23E-13
Fhl1	four and a half LIM domains 1	1.22	5.56E-07	-0.84	3.40E-04

Top 100 of significantly different mRNAs with reverse regulation between the three groups (Sham WT, TAC WT and TAC KO) and a minimum FC of 1.5 are displayed. Fold change and p-value is given for Sham WT vs TAC WT and TAC WT vs TAC KO. One-way Anova.

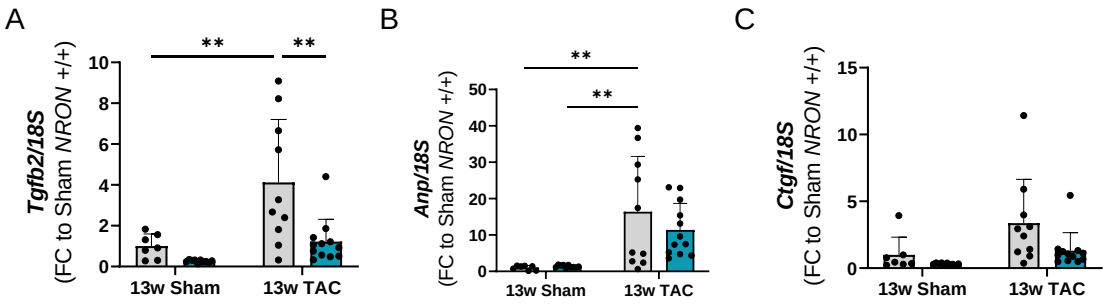

Figure S2: Validation of targets from transcriptomic data. RNA level of (**A**) *Tgfb2,* (**B**) *Anp* and (**C**) *Ctgf* mRNA after 13 weeks of surgery was measured by qPCR and normalized to 18S RNA. All data are mean ± S.D.; n=7-12. *P<0.05; **P<0.01; ***P<0.001; ****P<0.0001. Two-way ANOVA with Tukey's multiple comparisons test

Table S5: Primer sequences used for gene expression analysis.

Gene	Forward primer sequence	Reverse primer sequence
Gapdh	5'TTCACCACCATGGAGAAGGC3’	5'GGCATGGACTGTGGTCATGA3'
ActB	5'ATCAAGATCATTGCTCCTCCTG3'	5'AGGGTGTAAAACGCAGCTCA3'
18S	5'GTAACCCGTTGAACCCCATT3'	5'CCATCCAATCGGTAGTAGCG3'
Nron	5'AATGGTGCAGCTCGGATTAC3'	5'GGGAAGGGGTTAAGGTGGTA3'
Bnp	5'CTGAAGGTGCTGTCCCAGAT3'	5'GTTCTTTTGTGAGGCCTTGG3'
Mcip1.4	5'AGGGACTTTAGCTACAATTT3'	5'TATGTTCTGAAGAGGGATTC3'
Xist	5'TCATCCGCTTGCGTTCATAG3'	5'GAGATCAGTGCTGGCTAAATCAGA3'